A Super-Resolution Feasibility Study in Small-Animal SPECT Imaging

José L. Villena, Eduardo Lage, Álvaro de Carlos, Gustavo Tapias, Alejandro Sisniega, *Student Member IEEE*, Juan José Vaquero, *Senior Member IEEE*, Manuel Desco

***Abstract*– Lack of spatial resolution is a major drawback in small-animal SPECT imaging, particularly when parallel hole collimators are employed. This work evaluates the feasibility of enhancing the spatial resolution of a small-animal SPECT scanner by applying an approach based on a super-resolution technique combined with dedicated hardware . The detectors are based on PS-PMTs (Hamamatsu, H8500), NaI(Tl) crystal arrays and parallel hole collimators. The system enables the mechanical shifting of the gamma-cameras and the object under study during the acquisition in steps smaller than the detector intrinsic sampling pitch. This fact allows using a super-resolution technique without the necessity of blind movement estimators between projections. In the absence of noise the algorithm converged to the original image, and with real noisy data it achieved improvements in resolution between 28% (tomographic) and 42% (planar) in phantom studies.**

I. Introduction

SPATIAL resolution in SPECT systems with parallel hole collimation is limited by many physical parameters, especially when applied to small-animal imaging. This problem is usually overcome by using detectors based on pinhole collimators [1-2] with one or more apertures, thus achieving even sub-millimetric spatial resolution. However, with this configuration the geometric efficiency of the detector and the FOV size are strongly affected by the source-to-collimator distance, which is a major drawback of pinhole collimation using small-area detectors. More recently, super-resolution approaches have come up as an alternative to overcome the limits imposed by image sensors and therefore they can represent a low-cost solution to enhance spatial resolution in clinical nuclear medicine equipments [3], having already demonstrated satisfactory results in clinical PET imaging [4-5].

The term super-resolution (SR) commonly refers to the reconstruction process in which it is possible to obtain reconstructed images with better resolution than that provided intrinsically by the detector, by means of combining sets of images of the same scene slightly displaced from each other. The methodology proposed in this work is based on the acquisition, at each angular position of the detector, of projection sets from differents points of view (POVs) with relative displacements smaller than the detector intrinsic pitch. Projection sets are then combined into high-resolution sinograms by means of an iterative algorithm which accounts for the additional information provided by shifted projections from the same detector angular position.

The limits for quality and spatial resolution achievable using this kind of technique depend basically on the signal-to-noise ratio (SNR) of the acquired images and the intrinsic characteristics of the detection system.

In this work, we study the feasibility of an SR technique applied to a dedicated small-animal SPECT scanner, both on simulated and real data.

II. Material and Methods

A. Hardware

We have developed a small animal SPECT prototype based on a detection system consisting of two opposite gamma-cameras. Detectors include a position sensitive photomultiplier tube (Hamamatsu H8500, ~45x45 mm^2 effective area), a 30x30 pixelated scintillator array with elements of 1.4 x 1.4 x 6 mm^3 (1.6mm pitch) and appropriate electronics for matching the output signals from the detector to the data acquisition system. Each detector is assembled in a lead-covered case, as shown in Figure 1.

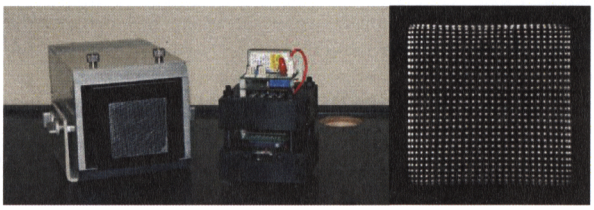

Fig. 1. Left: Lead-covered case of one of the detectors which contains the exchangeable collimator. Center: detector module with the NaI(Tl) scintillator crystal, PMT and read-out electronics. Right: field flood image of one detector obtained with ^{99m}Tc.

The design of the case includes the possibility of changing the collimator (pinhole or parallel hole, depending on the study requirements).

Detectors are attached to the gantry shown in Fig. 2. The system offers 6 motorized movement axes controlled by a computer by means of RS-232 communication and intelligent servo drives. The available axes are the following:

1. *Bed*: Allows movements of the sample along the axial direction (Z axis Figure 2).

Manuscript received November 14, 2008. This work is partially funded by the CD-TEAM Project, CENIT Program, Spanish Ministerio de Industria, and with grants from the Ministerio de Educación y Ciencia, projects TEC2007-64731 and TEC2008-06715-C02-01.

José Luis Villena, Eduardo Lage, Álvaro de Carlos, Gustavo Tapias, Alejandro Sisniega, Juan José Vaquero and Manuel Desco are with the Unidad de Medicina y Cirugía Experimental, Hospital General Universitario Gregorio Marañon, Madrid, Spain. (Corresponding author phone: +3491586667, email: desco@mce.hggm.es).

2. *Ring*: Allows movements of the detectors around the sample.
3. *Axes movement on X direction (transaxial)*: This motorized stage is attached to the ring, and allows radial movements (X direction) of the detectors.
4. *Axes movement on Y direction (transaxial)*: This motorized stage is assembled on the previously described one, and provides mobility of the detector in the Y transaxial direction.

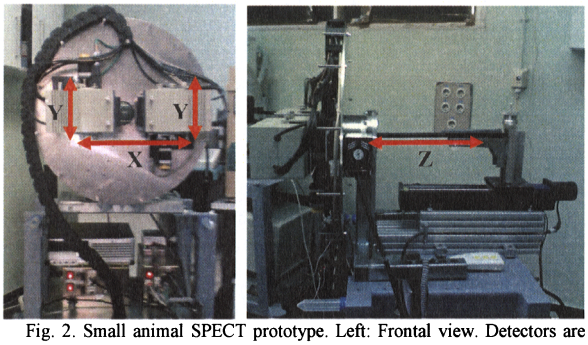

Fig. 2. Small animal SPECT prototype. Left: Frontal view. Detectors are mounted on motorized stages which allow its movement in the transaxial plane. Right: Side view. The object under study is placed on a bed allowing sub-millimetric displacements in the axial direction.

B. Software

The image processing is based on the algorithm proposed by Irani & Peleg [5]. The original procedure includes a method to estimate the movement between the different images corresponding to the same scene. However, motion estimation is not required in our implementation as scene shifts are known a priori.

Irani & Peleg algorithm was intended for 2D images while SPECT imaging is three-dimensional by nature. It is possible to use different formats to represent the acquired data, depending on the sorting criterion used. Among all, the sinogram representation is the one which best fits the movement system implemented, because shifts on the tangential axis represent the upsampling of each row in the sinogram, and shifts along the bed axis increase the number of slices in the sinogram. In this way, our implementation was designed to operate with sinograms instead of reconstructed SPECT images.

To better understand the algorithm we will describe in more detail the movement sequence executed at each angular position during a tomographic acquisition. Fig. 3 shows four different POVs corresponding to different positions in Y or Z directions of the detector or object under study. For simplicity the detector in Fig. 3 is represented as a 2x2 array and the object under study is represented by a grey circle. These positions define transformations T_k, where the suffix k (k=1,2,…K) refers to the different views of the scene, representing the image translation from POV 1 to POV K. In this work we use a number of k=4 POVs.

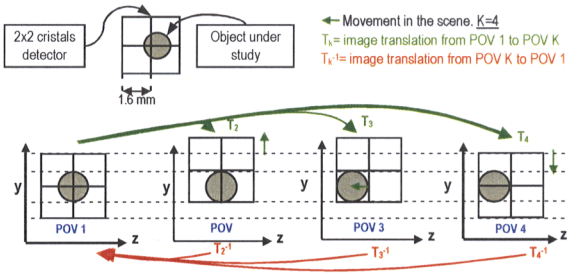

Fig. 3. Movements in acquisition, POVs generated and transformations T_k and T_k^{-1} related to the shifts.

Once acquisition is completed, the following step is to generate a set of low-resolution (LR) sinograms (g_k) corresponding to each POV (Fig. 4). Applying formula (1) to these LR sinograms we obtain an initial guess for a high-resolution (HR) sinogram (f_0), whose improvement is the goal of the iterative algorithm. The $\uparrow s$ operator in (1) and (3) represents the up-sampling of the LR sinograms by splitting each pixel by a factor equal to the number of steps performed during acquisition. The term T_k^{-1} represents the shift of the HR form of the sinogram to a common HR reference which, in this case, coincides with POV 1.

The next step of the algorithm produces a set of synthetic LR sinograms (g_k) from the initial guess of the HR sinogram by applying the transformations T_k and the $\downarrow s$ operator. The down-sampling of a HR sinogram into a LR sinogram is done in this case by averaging the HR pixels which correspond to an original LR pixel (2). The difference between this synthetically generated set of LR sinograms and the actually acquired set of sinograms is used to update the solution by adding (3) to the current HR sinogram to obtain the next estimation (4).

For simplicity, in our implementation, both the h function in (2) (detector PSF or blur kernel) and the p function in (3) (the inverse of the blurring kernel h) were taken as one-pixel width 'delta' functions. In this way they do not change the results, but we have kept them in the flowchart to allow for possible future improvements.

The process is repeated iteratively (n times) until a maximum number of iterations is reached. Finally, to obtain the final SPECT image with the expected better resolution, the generated HR sinograms are reconstructed by means of a Filtered Backprojection (FBP) algorithm with a ramp filter (cut-off frequency = 0.5).

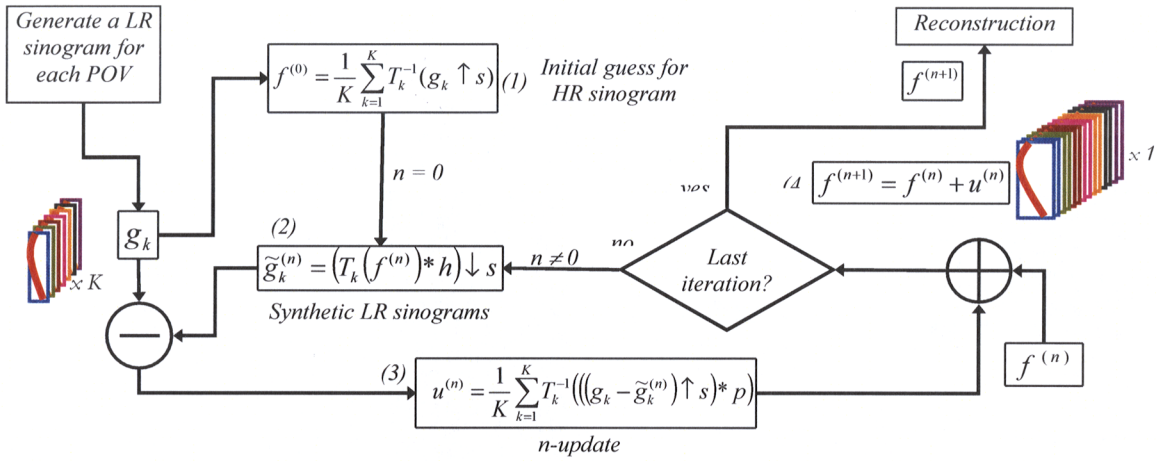

Fig. 4. Flowchart of super-resolution algorithm implementation.

Shifts between acquired images at the same angular position must be smaller than the detector intrinsic sampling pitch, in such a way that the acquired dataset provides additional information over that existing in the LR data. Using K steps in acquisition, the theoretical expected improvement in resolution is $\sqrt{K}$ because we virtually split the detector into elements with sampling pitch $\sqrt{K}$ times smaller than the original. Therefore, in the case of 4 steps the theoretical factor for improving resolution is two.

III. Preliminary Results

A. Synthetic data

We tested the algorithm with different synthetic 2D images. In our implementation of the algorithm, the bidimensional or planar case represents a particular situation with respect to the tomographic acquisition, in which we only acquire N=1 angular positions. The synthetic HR planar image generated consisted of six capillary sources of 1mm diameters placed as shown in Fig. 5. We simulated the acquisition of 4 LR images by means of 4 displacements and down-sampling of each translated image, modeling in this way an ideal detector with spatial resolution twice worse than the original image.

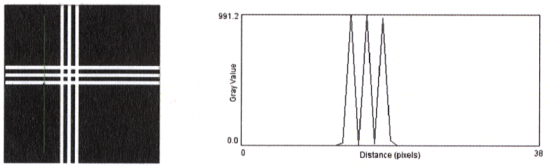

Fig. 5. Synthetically generated high-resolution image. Each simulated capillary source is 1mm-width (1 pixel).

In the absence of noise, the algorithm converged to the original image (Fig. 6) approximately after 200 iterations. Fig. 6 also shows a profile drawn both in the initial guess and in the final iteration.

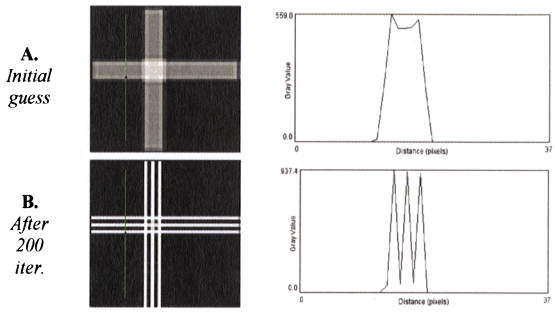

Fig. 6. **A.** Initial HR image from which the algorithm begins to iterate. **B.** HR image after 200 iterations.

To check the algorithm performance on noisy data, we added white noise to the original HR image. Fig. 7 represents the output when the original image has a SNR=2.5 (4 dB). To calculate the SNR we divided the squared number of total counts in the image without noise by the square of the total counts in the added noisy image. When the SNR decreases, we observe how the algorithm is not able to converge to the exact solution although it still achieves reasonable results. Note that image noise is also enhanced throughout this process.

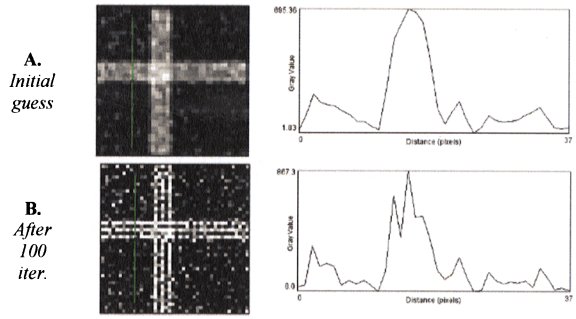

Fig. 7. **A.** Initial HR image from which the algorithm begins to iterate. **B.** HR image after 100 iterations.

B. Real data

We tested the algorithm by acquiring four scans of a cross-shaped phantom (Fig. 8.A), which consisted of four capillary sources filled with a solution of Tc^{99m}. There was an empty capillary between the hot sources.

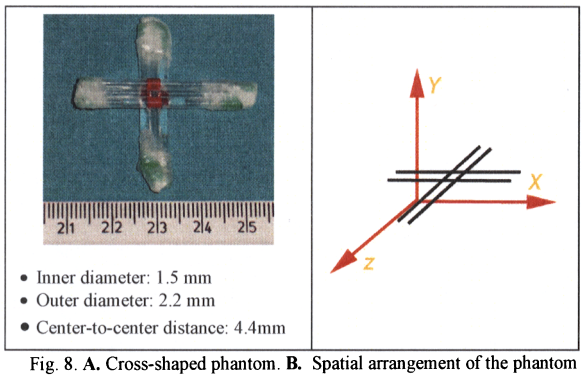

Fig. 8. **A.** Cross-shaped phantom. **B.** Spatial arrangement of the phantom in the tomograph reference system.

Each scan combined two features chosen between the following pairs: planar/tomographic imaging and conventional (No-SR)/super-resolution (SR) acquisition. Studies parameters are shown in Table 1. In the scans labeled as 'SR' both detectors and phantom were shifted according to the movements explained in Fig. 3. Although the system provides two detector heads, for these preliminary tests only data from one head were processed.

	No-SR	SR
Planar • **N=1 angular position** • **Coronal view** • **Distance to COR= 6 mm**	**720 s/proy**	**4 POVs 180 s/POV**
Tomographic • **N=90 angular positions** • **Circular orbit over 360°** • **Distance to COR =26 mm**	**80 s/proy**	**4 POVs/angular pos 20 s/POV**

Table 1. Parameters of the phantom studies acquired.

Planar imaging

Figure 9 shows the coronal view of the phantom and profiles across the images in three cases:

1. Top. The projection obtained from the No-SR scan.
2. Middle. The projection obtained by merely correcting the data from the SR scan according to (1), i.e. the initial guess.
3. Bottom. The projection obtained after 4 complete iterations of the SR algorithm.

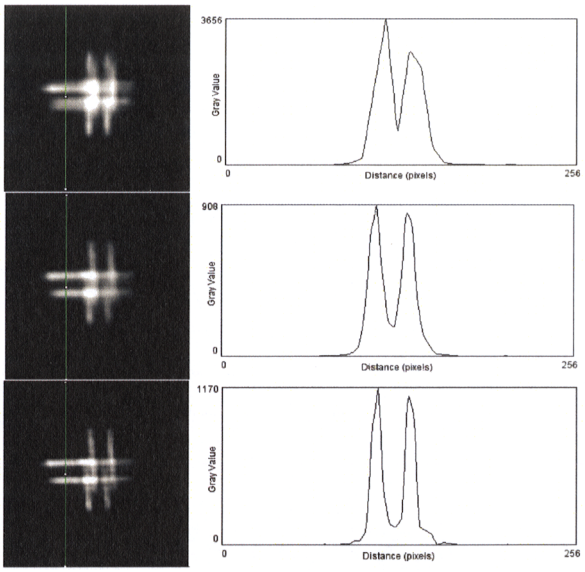

Fig. 9. Results in planar imaging with real data. **Top.** No SR applied. **Middle.** Initial guess. **Bottom.** After 4 SR iterations

We observe a resolution enhancement from the top to the bottom in Fig. 9. In order to quantify this improvement we measured a mean FWHM by fitting the profiles to Gaussian functions (Table 2).

	Without Super-R	Initial guess	4 iterations
FWHM (mm)	**2.70**	**2.34**	**1.55**

Table 2. Spatial resolution (mean FWHM) obtained by fitting the profiles to a Gaussian function

Tomographic imaging

In the SR-tomographic scan we obtain 4 LR sinograms. The super-resolution algorithm was applied to the 4 data sets, obtaining a HR sinogram afterwardsreconstructed with an FBP algorithm.

Observe in both figures 10 and 11 how capillaries can easily be identified after 4 iterations. For each X, Y and Z directions, spatial resolution was computed as the average FWHM by fitting to Gaussian functions. The improvement in resolution is presented in table 3.

		Without S-R	Initial guess	4 iterations
FWHM (mm)	**Y direction**	**4.6**	**3.7**	**3.3**
	X direction	**Not Resolved**	**4.4**	**3.7**
	Z direction	**4.5**	**3.7**	**3.2**

Table 3. Comparative values of transaxial and axial spatial resolution (mean FWHM) extracted from the profiles, traced in y, x and z directions for each capillary, fitted to a Gaussian function.

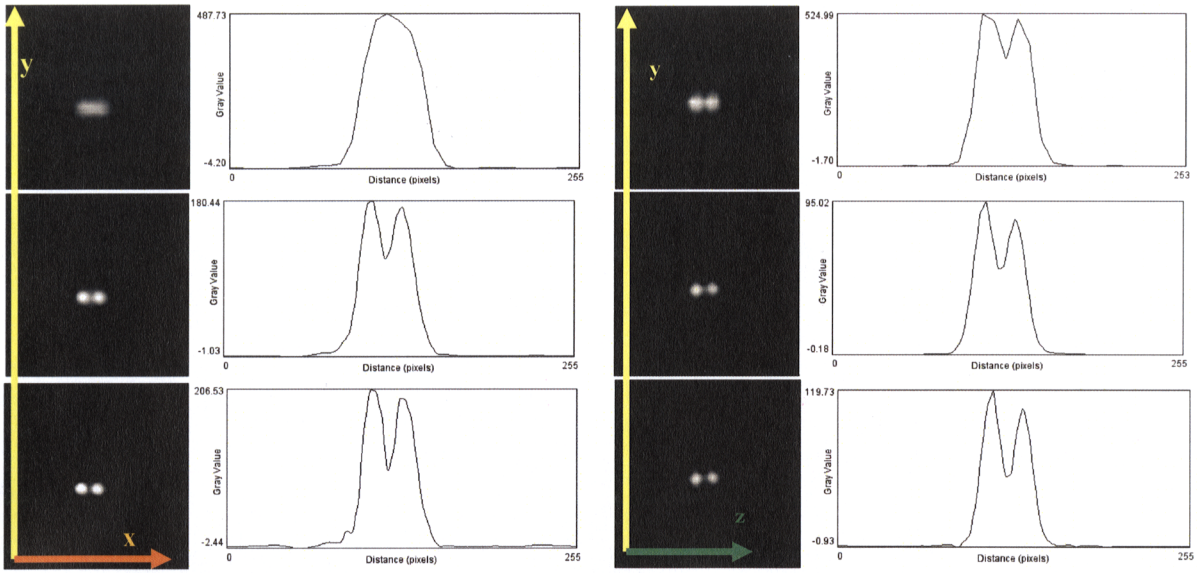

Fig. 10 (left) and 11 (rigth) shows the same reconstructed axial slice, relative to the three cases already mentioned in planar imaging, and the profiles traced across the two capillaries (along x and z direction). **Top.** No SR applied. **Middle.** Initial guess. **Bottom.** After 4 SR iterations

IV. Discussion And Conclusions

To our knowledge, there is no other published work using a super-resolution approach in small-animal SPECT imaging. However, it has been showed in clinical PET that a similar approach can improve spatial resolution by 9%-52% [4]. This result is consistent with the ones found in our work for small-animal SPECT.

As expected, the proposed method improves the spatial resolution, but also enhances noise and artifacts. This effect becomes more noticeable as the number of iterations increases.

Preliminary results show that the super-resolution approach can be applied to small animal SPECT imaging, noticeably improving the spatial resolution achievable with parallel hole collimation. Determination of the optimum trade-off between acquisition time and resolution enhancement requires further investigation.

Acknowledgment

We thank the technician Alexandra de Francisco for his support on the phantom studies.

References

[1] F. Garibaldi, et.al, "Small Animal Imaging by Single Photon Emission Using Pinhole and Coded Aperture Collimation", IEEE Trans. Nucl. Sci., vol. 52, no. 3, pp. 573-579, 2005.

[2] Tsutomu Zeniya, et.al, *"Use of a Compact Pixellated Gamma Camera for Small Animal Pinhole SPECT Imaging"*, Annals of Nuclear Medicine, vol. 20, no. 6, pp. 409-416, 2006.

[3] F. J. Caramelo, G. Almeida, L. Mendes and N.C. Ferreira. *"Study of an iterative super-resolution algorithn and its feasibility in high-resolution animal imaging with low-resolution SPECT cameras"*. IEEE Nucl. Sci. Symposium Conference Record, pp. 4452-4456, 2007.

[4] J.A. Kennedy, O. Israel, A. Frenkel, R. Bar-Shalom and H. Azhari. *"Super-Resolution in PET Imaging"*. IEEE Trans. Nucl. Sci., vol. 25, no. 2, pp. 137-147, 2006.

[5] J.A. Kennedy, O. Israel, A. Frenkel, R. Bar-Shalom and H. Azhari. *"Improved Image Fusion in PET/CT Using Hybrid Image Reconstruction and Super-Resolution"*. International Journal of Biomedical Imaging, vol. 2007, Article ID 46846.

[6] M. Irani, S. Peleg. *"Motion analysis for image enhancement: resolution, occlusion, and transparency"*. J. Vis. Commun. Image Rep., vol.4, no. 4, pp. 324-335, 1993.